Inorganic Chemistry

Article

pubs.acs.org/IC

High Temperature X-ray Diffraction Study of the Oxidation Products and Kinetics of Uranium−Plutonium Mixed Oxides

Michal Strach,*[,†,‡] Renaud C. Belin,*[,†] Jean-Christophe Richaud,[†] and Jacques Rogez[‡]

[†]CEA, DEN, DEC, SPUA, LMPC, Cadarache, F-13108 Saint-Paul-Lez-Durance, France

[‡]IM2NP, UMR 6122, CNRS, Aix Marseille Université, Case 251, Avenue Escadrille Normandie Niemen, 13397 Marseille Cedex 20, France

ABSTRACT: The oxidation products and kinetics of two sets of mixed uranium−plutonium dioxides containing 14%, 24%, 35%, 46%, 54%, and 62% plutonium treated in air were studied by means of in situ X-ray diffraction (XRD) from 300 to 1773 K every 100 K. The first set consisted of samples annealed 2 weeks before performing the experiments. The second one consisted of powdered samples that sustained self-irradiation damage. Results were compared with chosen literature data and kinetic models established for UO_2. The obtained diffraction patterns were used to determine the temperature of the hexagonal M_3O_8 (M for metal) phase formation, which was found to increase with Pu content. The maximum observed amount of the hexagonal phase in wt % was found to decrease with Pu addition. We conclude that plutonium stabilizes the cubic phases during oxidation, but the hexagonal phase was observed even for the compositions with 62 mol % Pu. The results indicate that self-irradiation defects have a slight impact on the kinetics of oxidation and the lattice parameter even after the phase transformation. It was concluded that the lattice constant of the high oxygen phase was unaffected by the changes in the overall O/M when it was in equilibrium with small quantities of M_3O_8. We propose that the observed changes in the high oxygen cubic phase lattice parameter are a result of either cation migration or an increase in the miscibility of oxygen in this phase. The solubility of Pu in the hexagonal phase was estimated to be below 14 mol % even at elevated temperatures.

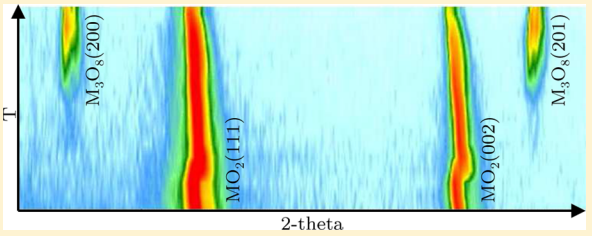

INTRODUCTION

Uranium−plutonium mixed oxides with high plutonium content are considered as candidates for fuel used in the IVth generation of nuclear reactors.[1] The ternary system U−Pu−O has been extensively studied for a range of compositions and at various temperatures, but still, data on some domains remains scarce. Numerous studies have been conducted in the PuO_2−UO_2−Pu_2O_3 region,[2−9] leading to a fairly good understanding of the hypo-stoichiometric part of the phase diagram. The development of this type of fuels also requires studying the oxidation products and kinetics for the purposes of fuel elaboration methods, better understanding and modeling of long-term storage,[10−12] behavior under accident conditions,[1] fuel−cladding interactions and predicting fuel restructuring. It has been shown that the oxidation of UO_2 produces higher oxides, such as U_4O_9, U_3O_7, and U_3O_8, depending on temperature and oxygen potential.[13,14] Judging by the results of previous studies,[2,15] the U−Pu−O system, with small additions of Pu, up to 20−30%, exhibits similar behavior and can present a wide range of nonstoichiometry for all compositions. Since physical and chemical properties change with the O/M ratio and are different for each oxidation product,[11,13] it is crucial to determine precisely the phase boundaries and oxidation mechanisms in the hyperstoichiometric region UO_2−PuO_2−U_3O_8.

It has been well-established that materials containing fissile isotopes evolve during storage due to self-irradiation induced defects. These defects include He trapped in a vacancy and cation and anion Frenkel defects and might induce changes in properties of the material such as decrease in the thermal conductivity or expansion of the lattice parameter.[16] Studying the influence of autoirradiation on the evolution of materials is of importance as usually the samples are stored for a significant amount of time between fabrication and carrying out experimental work.

In this study, the crystallographic phases of U−Pu−O powders with and without self-irradiation defects were studied by means of high temperature X-ray diffraction, during thermal treatment under air. All samples were prepared from an initial batch of stoichiometric $(U_{1-y},Pu_y)O_2$ pellets. On the basis of the obtained results, we have discussed the impact of different plutonium contents and self-irradiation defects on the behavior of the studied dioxides during oxidation in synthetic air. To our knowledge, this is a first attempt to study in situ the oxidation products and kinetics of annealed and self-irradiated mixed U−Pu oxides with such high plutonium contents.

MATERIALS AND METHODS

The powders used in this study, with Pu contents of 14, 24, 35, 46, 54, and 62 mol % (MOX14−MOX62), were prepared by crushing sintered stoichiometric pellets of the composition $(U_{1-y},Pu_y)O_2$. These pellets were fabricated from cogrinded UO_2 and PuO_2 powders.

Received: July 8, 2014
Published: November 20, 2014

   dx.doi.org/10.1021/ic501580x | Inorg. Chem. 2014, 53, 12757−12766

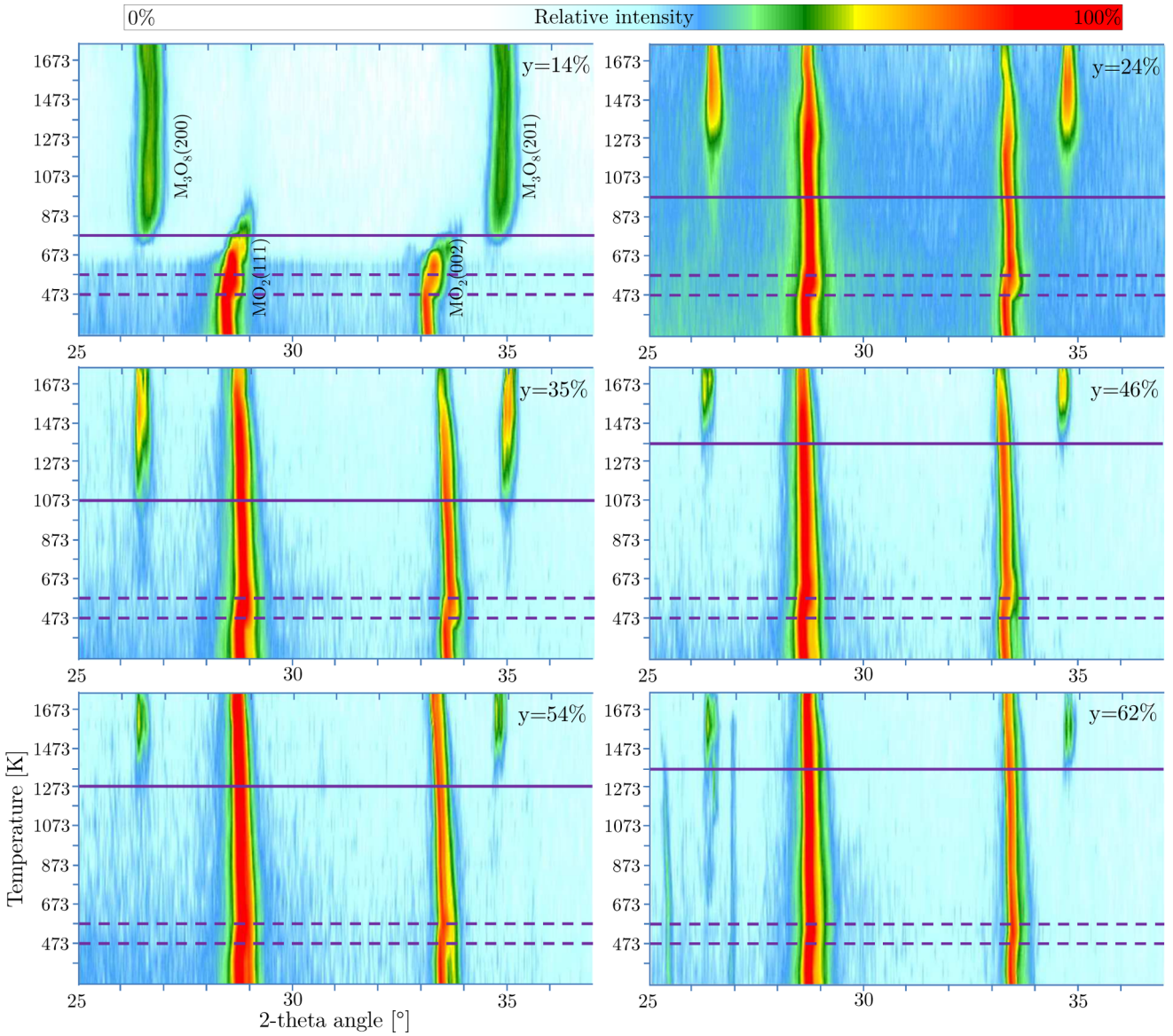

Figure 1. Isointensity maps of all oMOX samples in the angular interval 25° < 2θ < 37°. The region delimited by the two dashed horizontal lines shows the temperature interval at which the oxidation begins. The solid lines show the temperatures at which the M_3O_8 phase started forming.

Stoichiometry was achieved by sintering the materials under a given oxygen potential, which, in turn, was done by adjusting the moisture content of the gas entering the furnace. The fabrication process was described in detail by Truphémus et al.[4] Pu content was determined by potentiometric titration performed five times for each sample. The samples were stored in a glovebox, which was kept under nitrogen atmosphere with ∼50−100 ppm of water vapor for between 650 and 950 days after fabrication. Experiments were carried out on two sets of samples. Samples in the first set were prepared using the initial pellets, annealed at around 1273 K for 10 h under Ar + H_2 + 10 000 ppm of H_2O vapor, and then slowly cooled to room temperature 2 weeks before the diffraction patterns were acquired. An appropriate thermal profile and atmosphere were chosen, with a temperature high enough for the defects to relax, and the oxygen potential of the gas injected in the furnace corresponding to the oxygen potential of a stoichiometric $MO_{2.00}$. These samples were designated as aMOX. The second set comprised six untreated, powdered samples stored in a glovebox under the mentioned conditions, designated as oMOX.

The oxidation was observed in situ by X-ray diffraction. The equipment used was a Bragg−Brentano θ−θ BRUKER D8 Advanced X-ray diffractometer with copper radiation from a conventional tube source (Kα_1 + Kα_2 radiation, λ = 1.5406 and 1.5444 Å). The pressure inside the sample chamber was estimated to be 1.2 atm. During all experiments flow rates were kept at around 5 L/h, and the gas used was synthetic air with an amount of water vapor considered insignificant (∼5 ppm). Heating was achieved by applying electrical current across a metallic strip upon which the powdered material was spread. All the experiments described in this study were done with two Pt heating strips: one for oMOX and one for aMOX. To learn the difference between the temperature measured by a thermocouple placed underneath the heating strip and the real temperature experienced by the sample, MgO was heated up to 1773 K, and the changes of its lattice parameter were compared to values given by the equipment manufacturer and available in ref 17. The procedure was repeated several times. The dependence was noted and the uncertainty estimated at ±15 K.

Pellets were crushed in an agate mortar, and the resulting powder (∼50 mg) was immediately inserted on the Pt heating strip. Small quantities of ethanol were added to each powder to evenly distribute it on the heating strip and avoid scattering. Rocking curve procedure and Z adjustment were performed prior to any experiment to determine the angular position and displacement. The samples were heated to around 1773 K, with an XRD scan each 100 K beginning at room temperature and followed by 373 K. Patterns were acquired between

dx.doi.org/10.1021/ic501580x | Inorg. Chem. 2014, 53, 12757−12766

Table 1. Key Characteristics of All the Studied Samples[a]

				lp at 573 K [Å]			
name	Pu/M [mol %]	$T_{M_3O_8}$ [K]	starting lp [Å]	MO_2	MO_{2+x}	T_r	M_3O_8 max wt %
oMOX14	14	773	5.4644	5.4781	5.4554		100
aMOX14	14	773	5.4592	5.4691			100
oMOX24	24	973	5.4594	5.4759	5.4540	873	62
aMOX24	24	1073	5.4526	5.4663	5.4457		52
oMOX35	35	1073	5.4516	5.4681	5.4475	973	43
aMOX35	35	1173	5.4441	5.4596	5.4401		43
oMOX46	46	1373	5.4460	5.4616	5.4446	973	40
aMOX46	46	1273	5.4381		5.4377		40
oMOX54	54	1273	5.4384	5.4539	5.4347	1073	22
aMOX54	54	1273	5.4306		5.4342		28
oMOX62	62	1373	5.4337	5.4488	5.4394	1173	20
aMOX62	62	1373	5.4241		5.4314		22

[a] $T_{M_3O_8}$ is the temperature of the hexagonal phase formation. Starting lp is the lattice parameter measured at room temperature, before the heat treatment. Lp at 573 K specifies the lattice parameters of the cubic phases or phase at the indicated temperature. T_r (r = relaxation) is the temperature at which the oMOX and aMOX lattice parameters align. M_3O_8 max wt% is the highest observed amount of the hexagonal phase for each sample.

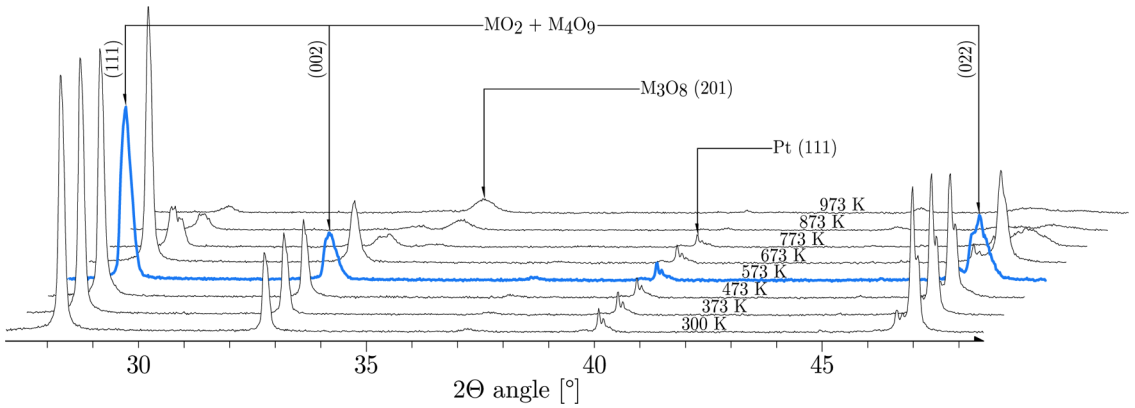

Figure 2. XRD patterns of aMOX14 for an angular range 28° < 2θ < 48° between 303 and 973 K. The pattern taken at 573 K was marked in blue and bold and was fitted using two cubic structures. Reflections corresponding to the observed structures were labeled with the adequate (*hkl*) planes in brackets.

25° < 2θ < 140°, by moving the source and detector at 0.02°/0.3 s, thus achieving a full scan in around 24 min. The heating rate between each step was 5 K/s. Before each scan, a delay of 2 min was imposed to achieve stabilization. This resulted in an approximate overall heating rate of 4°/min. The lattice parameter evolution is plotted against temperature in all figures, but the temperature−time dependence is linear; thus, time evolution can be also discussed on the basis of the same plots.

TOPAS 4.0[18] software was used to analyze the acquired patterns. The instrument contributions such as the geometry, tube type, and slits were included in the fitting according to the fundamental parameter approach.[19] The Rietveld method[20] was used to fit all recorded patterns. The background noise was approximated by a Chebyshev function with 3 terms. Contributions from the microstructure were simulated by a physical broadening function. The error in the lattice parameter value was estimated to be 10^{-3} to 10^{-2} Å, depending on the intensity of the peaks of the considered phase. The error on the weight % from Rietveld analysis is estimated at ±5 wt % by the software, which indicates that when the ratio between the phases is far from 50/50, the relative uncertainty is significant. When the amounts of the present phases are comparable, we estimate the error at ±7 wt %.

RESULTS

Oxidation products were studied on the basis of the XRD data analysis. The diffraction patterns, obtained during each temperature treatment for oMOX samples, were put together to create isointensity maps shown in Figure 1. The specific angle range in this figure was chosen as it includes peaks of all of the present phases, and thus it enables following the structural changes. The isointensity maps for the annealed samples do not differ strongly from the ones presented here. The slight differences were noted upon close examination of each pattern and are discussed later. The temperatures indicating significant events for all the studied samples were discussed in the Structural Changes section. Additionally, the lattice parameter evolution with temperature was evaluated for the observed cubic structures and is discussed in the Evolution of Lattice Parameter section. The lattice parameters of the hexagonal M_3O_8 structure present in the acquired patterns were not evaluated in this study, but it was used in the refinement and its weight % evolution with temperature is described in the M_3O_8 wt % Evolution section. The key characteristics of the studied samples are listed in Table 1.

Structural Changes. The earliest structural change was observed in the pattern taken at 573 K with the distortion of

dx.doi.org/10.1021/ic501580x | Inorg. Chem. 2014, 53, 12757−12766

the cubic structure peaks, visible for the (111) and (002) reflections for all samples. This distortion manifested in a noticeable decrease in the intensity of the reflections, which can be observed in Figure 2. These distorted reflections were successfully fitted using two cubic-type structures in the case of aMOX24 and aMOX35 and all the aged samples. One was designated as MO_2, and the other as MO_{2+x}. After this event, at 673 K and above, only one cubic structure was observed for all samples. As the temperature increased, the samples oxidized further, and a hexagonal M_3O_8 structure appeared. The temperature designated as the beginning of the hexagonal phase formation ($T_{M_3O_8}$ in Table 1) was determined by finding the pattern where the low-angle hexagonal reflections started to be clearly distinguishable from the background. This temperature increased with Pu content, and at the same time, the maximum observed intensities of the hexagonal reflections diminished. Only for samples containing 14 mol % Pu has the M_3O_8 phase almost completely replaced the cubic phase. For all the other samples, the cubic structure was observed up until the maximum temperature with fairly intense reflections.

Evolution of the Lattice Parameter. Evolution of the cubic structure lattice parameter in temperature was plotted for samples MOX24−MOX62 in Figures 3−7. The fitting was

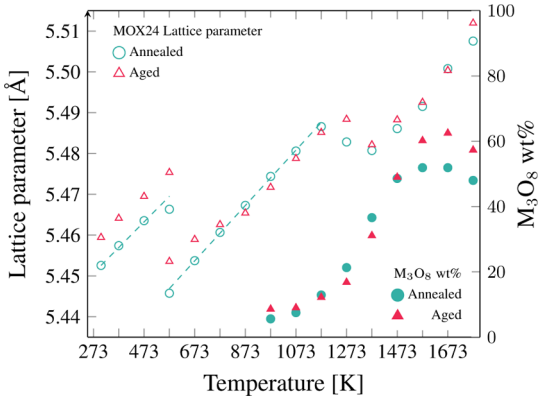

Figure 3. Evolution of the lattice parameter of the cubic phase and the M_3O_8 phase fraction as a function of temperature for samples containing 24 mol % Pu. Dashed line: linear part or the annealed sample lattice parameter evolution. Here, two cubic phases were observed for both samples at 573 K. When the hexagonal phase content reaches 20 wt %, a decrease in the cubic lattice parameter can be observed for both samples (commencing earlier in the case of the annealed sample).

done using a $Fm\bar{3}m$ (space group 225) structure for the cubic phases and a $P\bar{6}2m$ (space group 189) structure for the hexagonal phase with the atomic sites determined by Desgranges et al.[21] for the U−O system. The cubic phase with an O/M close to 2.25 has been determined to be I-centered cubic M_4O_9,[24] but it is still not certain whether it is truly so. The seemingly well-established belief that oxygen interstitials form clusters within the lattice to later form a distinct structure[22] was questioned by Conradson et al.[23] on the basis of high-quality XAFS results. The difference between this phase and the fluorite MO_2 is mostly in the oxygen atomic positions while the metal lattice remains relatively unchanged, hence our choice to fit it with the $Fm\bar{3}m$ structure. With the resolution of our experimental technique, it is impossible to observe the very slight modifications of the oxygen sublattice,

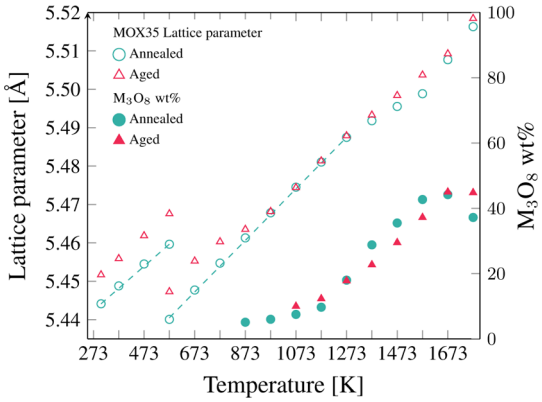

Figure 4. Evolution of the lattice parameter of the cubic phase and the M_3O_8 phase fraction as a function of temperature for samples containing 35 mol % Pu. Dashed line: linear parts or the annealed sample lattice parameter evolution. Here, two cubic phases were observed for both samples at 573 K. When the haxagonal phase content exceeds 20 wt %, a decrease in the cubic lattice parameter can be observed as in the case of MOX24 samples but less pronounced.

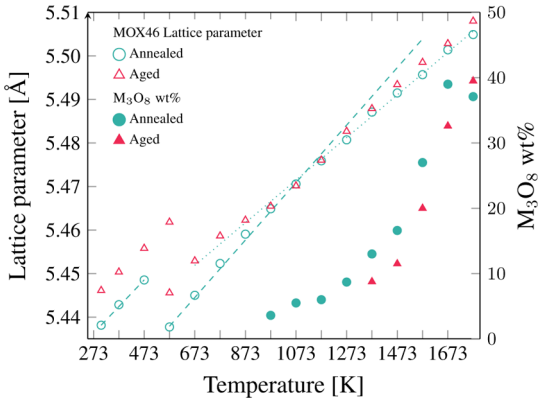

Figure 5. Evolution of the lattice parameter of the cubic phase and the M_3O_8 phase fraction as a function of temperature for samples containing 46 mol % Pu. Dashed line: initial linear part or the annealed sample cubic lattice parameter evolution with small quantities of M_3O_8. Dotted line: linear part or the annealed sample cubic lattice parameter evolution with quantities of M_3O_8 above 10 wt % (at $T >$ 1273 K). The departure from the initial line occurs earlier in terms of temperature and O/M than in the case of samples with lower Pu contents.

and thus, the $Fm\bar{3}m$ structure was successfully used to fit also the second cubic phase.

Annealed Samples. The evolution of the cubic structures' lattice parameters can be divided into two regions before large quantities of the M_3O_8 formed. We observed a linear increase at temperatures below 473 K, which was afterward followed by another linear segment with a slightly steeper slope, up to a certain temperature. All linear regression parameters can be found in Tables 2 and 3 ($a = m \times T + a_0$, where a is the lattice parameter, m is the slope, a_0 is the lattice parameter at 0 K, and R^2 is the coefficient of determination). The annealed aMOX14 sample has apparently converted to almost pure M_3O_8 very early, so the lattice parameter of the cubic structure at temperatures higher than 573 K is not discussed. The cubic lattice parameters for this sample at lower temperatures were plotted in Figure 8.

The cubic lattice parameter was affected by the formation of the hexagonal phase. What can be observed in Figure 3, for the

dx.doi.org/10.1021/ic501580x | Inorg. Chem. 2014, 53, 12757−12766

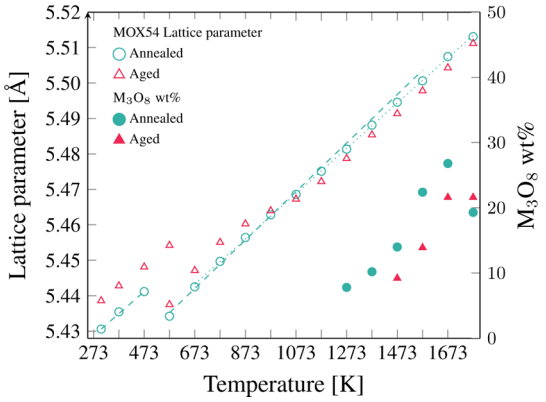

Figure 6. Evolution of the lattice parameter of the cubic phase and the M_3O_8 phase fraction as a function of temperature for samples containing 54 mol % Pu. Dashed line: initial linear part or the annealed sample cubic lattice parameter evolution with small quantities of M_3O_8. Dotted line: linear part or the annealed sample cubic lattice parameter evolution at $T > 1173$. The two linear slopes are only slightly different.

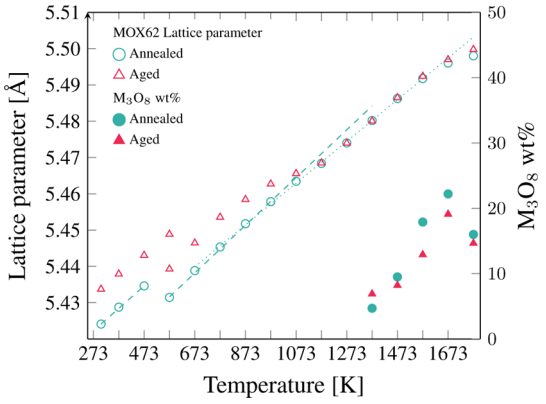

Figure 7. Evolution of the lattice parameter of the cubic phase and the M_3O_8 phase fraction as a function of temperature for samples containing 62 mol % Pu. Dashed line: linear part or the annealed sample lattice parameter evolution. Dotted line: linear part or the annealed sample cubic lattice parameter evolution at $T > 1073$.

Table 2. Linear Regression Parameters for Cubic Phase Lattice Constants Determined at Temperatures below 473 K for the Annealed Samples[a]

sample	m [10^{-5}]	a_0 [Å]	R^2
aMOX14	6.331	5.440	0.999
aMOX24	6.428	5.433	0.999
aMOX35	6.074	5.426	0.998
aMOX46	6.086	5.420	0.998
aMOX54	6.193	5.412	0.997
aMOX62	6.159	5.406	0.999

[a] $a = m \times T + a_0$, where a is the lattice parameter, m is the slope, a_0 is the lattice parameter at 0 K, and R^2 is the coefficient of determination.

annealed sample containing 24 mol % Pu, is that there is a strong decrease in the lattice parameter coinciding with an increase in the amount of the hexagonal phase to 20−30 wt %. Another interesting observation is that, for higher Pu contents, the linear evolution continues with a gentler slope after the content of the hexagonal phase rises to around 10 wt %, with a high R^2 value.

Table 3. Linear Regression Parameters for Cubic Phase Lattice Constants Determined at Temperatures above 473 K for the Annealed Samples[a]

sample	m [10^{-5}]	a_0 [Å]	R^2	T range [K]
aMOX24	6.784	5.408	0.998	573−1173
aMOX35	6.718	5.402	0.999	573−1273
aMOX46	6.936	5.398	0.996	573−973
aMOX54	6.842	5.396	0.996	573−1073
aMOX62	6.569	5.394	0.999	573−973

[a] $a = m \times T + a_0$, where a is the lattice parameter, m is the slope, a_0 is the lattice parameter at 0 K, and R^2 is the coefficient of determination.

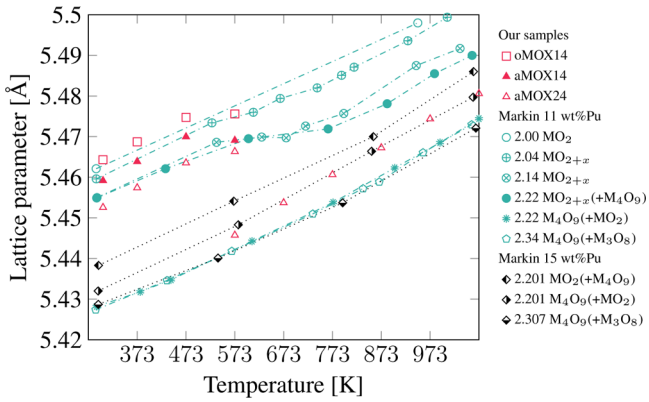

Figure 8. Comparison of the cubic lattice parameter temperature evolution of samples aMOX14 and aMOX24 with literature data.[2]

Aged Samples. Three regions before the M_3O_8 phase formation have been designated, due to apparent differences in the evolution. Below 473 K, the increase is linear for all oMOX samples. The starting lattice parameters indicate a departure from the expected value for newly fabricated, stoichiometric samples.

For sample oMOX14, large quantities of the hexagonal phase formed at 773 K resulting in significant swelling of the powder and making the analysis of the cubic phase lattice parameter impossible. Hence, the last registered lattice parameter corresponds to 673 K, and it would not be reasonable to discuss the evolution on the basis of just two points determined from patterns where the influence of M_3O_8 was already significant. The cubic lattice parameters of oMOX14 at low temperatures were plotted in Figure 8.

As for all the other samples above 573 K, the increase in the lattice parameter was parabolic until a temperature dependent on the plutonium content (T_r listed in Table 1). Further on, the evolution was linear. For sample oMOX24, the hexagonal phase started to form above 1273 K, which resulted in irregularities in the cubic lattice parameter evolution. Also, a slight change in the slopes of the linear evolution can be observed when large quantities of M_3O_8 formed, for samples with $y = 0.35$, 0.46, and 0.54.

M_3O_8 wt % Evolution. The wt % of the hexagonal phase was obtained from refining the acquired patterns with the Rietveld method. The results were presented in Figures 3−7. The maximum amount of M_3O_8 formed for a given sample was noted in Table 1. The increase was slow at the beginning, but afterward the value rose rapidly to slow down again at higher temperatures. At 1773 K for most of the samples, the value was found lower than that obtained for the pattern taken at 1673 K.

dx.doi.org/10.1021/ic501580x | Inorg. Chem. 2014, 53, 12757−12766

Residual Signal. Some residual signals were present due to the fact that there were only two heating strips used, one for all the aMOX and one for the oMOX samples. Thus, in some instances the strip remained polluted with the previous powder, which had strongly adhered to the surface due to the high temperatures. These signals were neglected in the analysis and, in all cases except two, disappeared at 573 K with the phase transformation. For aMOX14 this contribution was quite large and did not allow for a precise determination of the lattice parameters at 573 K. For aMOX35 there was some residual M_3O_8 remaining on the strip; thus, a slight signal from this phase was observed from the beginning of the thermal treatment.

DISCUSSION

Although the isothermal plateau duration at each temperature was about 25 min, on the basis of a few longer isothermal experiments lasting several hours carried out on the same samples, we treat the acquired cubic lattice parameter values at low temperatures as temporary characteristics resulting from inhibited matter transport within the material. It was found by Tennery and Godfery[25] that the thermal history of samples can have an impact on the final products of oxidation and O/M in the case of MOX. It was proposed that gradual heating might allow time for formation of second-stage nuclei, which in turn makes it possible for the sample to oxidize further. If true, this mechanism would create space for such interim states during oxidation; i.e., moving to the next step is not possible without passing through the former, which might be restricted to a certain temperature and oxygen potential range. This effect would be amplified by inhomogeneities in the studied materials, which might be significant depending on the fabrication process. The details of EPMA experiments carried out on a sample studied here (i.e., the plutonium distribution in the sample obtained from comilled powders for 1 h), were listed by Vauchy et al.[26] On the basis of these results we can state that the homogeneity level of our samples was high, but the differences in cation distribution cannot be neglected.

The results discussed here can be taken as representative of the behavior of MOX powders oxidized from an O/M = 2.00 to a given higher O/M at temperatures up to 1373 K with isothermal plateaus lasting from 25 min to 20 h (heating rates between 5 K/min and 5 K/h). Above 1373 K the samples were most likely close to equilibrium with the gas, and the results were not affected by any kinetic effects. The data recorded above 1373 K is thus representative of steady states, independent of thermal history (these results might depend on thermal history for faster heating rates).

In situ X-ray diffraction is a convenient and useful tool in the studies of long-range order evolution in temperature. However, it has to be kept in mind that the phenomena described in the following sections result from underlying atomic scale changes, the study of which requires dedicated experimental equipment.[27−29] Thus, the authors wish to emphasize that the presented description drawn from our results is not a complete one, and accounts for only a part of the phenomena taking place during the transitions in the studied multicomponent materials, which transpire in the long-range order. Also, a direct connection between our findings and the U−Pu−O phase diagram cannot be made; nevertheless, we might draw some indirect conclusions in this matter as the results depend on the phase diagram.

We first discuss the annealed samples. Observations concerning self-irradiation phenomena are listed at the end, in the Effects of Self-Irradiation section.

Lattice Parameter at Temperatures below 573 K. The lattice parameters of the two annealed samples aMOX14 and 24 were compared with values found by Markin and Street[2] in Figure 8. It has to be noted that this data concerns samples with approximately constant O/M, while in this study the samples were allowed to exchange oxygen with the gas. Nevertheless, it is plausible to state that a comparison can be made for temperatures lower than 473 K, as in this range the diffusion of ions is strongly inhibited and the O/M had seemingly remained constant with increasing temperature.[25] The slopes determined in this study are similar to the ones found by Markin and Street[2] for constant O/M (Figure 8), which confirms our assumption. Also, in support of this statement, by plotting the lattice parameter versus the Pu content, we observed that the slopes of lines that join points taken at the same temperatures lower than 573 K are equal to the one determined from Vegard's prediction at room temperature.

Lattice Parameter at Temperatures above 573 K. Above 473 K, all samples started to oxidize, though the exact temperature which can be assigned to the beginning of oxidation of each oxide cannot be determined, but the differences between them had to be lower than 100 K. For samples with Pu content 24 and 35 mol %, the first X-ray pattern after the beginning of oxidation, taken at 573 K, suggests the appearance of another cubic structure with a much lower lattice parameter, as mentioned before. The lattice parameters of these two phases are listed in Table 1.

For the rest of the samples, the pattern registered at 573 K cannot be fitted with two cubic structures, though the reflections are distorted and the intensities are lower than at neighboring temperatures.

What can be observed in Figure 8 above 573 K is that our aMOX24 points correspond to the ones found by Markin and Street[2] for a sample containing 15 wt % Pu with an O/M = 2.201 and attributed to the M_4O_9 phase in equilibrium with MO_{2+x}. This is true up to 1073 K. The fact that the two data sets are superimposed is of no scientific value and most likely is a result of differences in sample properties.

What is worth observing, though, is the fact that the evolution of our lattice parameter is linear with the same slope as found by Markin and Street.

We can state that in our study samples underwent continuous oxidation until at least 1673 K, as the amount of the hexagonal phase has been rising up to this temperature. Thus, the observation from Figure 8 is clear evidence for the MO_{2+x} lattice parameter independence of the overall O/M. Thus, this phase exists only in a narrow stoichiometric domain, at least for Pu contents up to 24 mol %. Furthermore, from our results it is clear that the slope of the cubic lattice parameter evolution with temperature for the aMOX24 sample does not change until 1173 K, which widens the temperature range in which this is true.

Above 573 K the increase of the lattice parameter of all annealed samples is linear, up to a certain temperature coincidental with the formation of large quantities of M_3O_8. For aMOX24, when the amount of the hexagonal phase exceeds 20 wt % at 1273 K, the lattice parameter drops rapidly and afterward continues to increase linearly from 1373 to 1773 K. For other samples a similar behavior was observed, with the slope becoming gentler. This might be caused by either the

dx.doi.org/10.1021/ic501580x | Inorg. Chem. 2014, 53, 12757−12766

increase in the O/M of the cubic phase or the migration of cations between the phases as only these two processes might result in a lower lattice parameter in our case.

We cannot completely rule out the possibility of the increase in O/M having an impact on the lattice parameter of the high oxygen cubic phase. At higher temperatures this phase might be able to incorporate more oxygen than the amount corresponding to an O/M ≈ 2.25, which is usually given as the limit. This would manifest in the observed decrease in the lattice parameter.

As for the cation migration hypothesis, the lattice parameter of the aMOX24 sample after the decrease at 1273 K arrives at almost the same value as we find for aMOX62 at this temperature. A quantitative analysis of the Pu content present in the two observed phases is not possible as no data on the lattice parameter of stoichiometric compounds with considered Pu contents is available in the literature, and surely, the aMOX62 sample was also affected by similar phenomena preventing us from estimating the composition of the cubic phase in this case. Nevertheless, this explanation has been explored in the literature.

Migration of Cations. Benedict and Sari[33] concluded that the M_3O_8 phase remains poor in plutonium and the actinide is mostly present in the cubic phase. Markin and Street[2] on the other hand observed that when M_4O_9 is in equilibrium with M_3O_8, the lattice parameter of the former is independent of the O/M and that the Pu/U ratio in the biphasic M_4O_9+M_3O_8 region remains constant for compositions with $y \leq 0.3$. This was supported by an observation that the cubic lattice parameter of their M_4O_9+M_3O_8 sample with an O/M = 2.42 after reduction to O/M = 2.00 obeyed Vegard's law. This would mean that cation migration does not occur in a part of the discussed domain. It is only valid if we consider that the hexagonal phase can incorporate up to 30 mol % of Pu, which was also proposed by Markin and Street but was contradicted by Sari et al.,[3] who limited this solubility to 6%. Here we also observe that even at 1773 K for samples containing 14 and 24 mol % Pu there are always traces of the cubic phase, thus we must disagree with Markin and Street and lean rather toward the value reported by sari et al. and state that the solubility of Pu in the hexagonal phase is most likely slightly below 14 mol %. At the same time, for all annealed samples we observe that the cubic lattice parameter evolution remains linear even when M_3O_8 starts forming, thus confirming Markin and Street's other observations, to a certain extent. When large quantities of the hexagonal phase were present though, the cubic lattice parameter seemed affected.

Markin and Street's experimental results might have been caused by inhomogeneities in their samples. The abundance of uranium in certain areas will enhance oxidation and allow for the formation of the hexagonal phase without the necessity of Pu migration. At a certain point though, a greater amount of M_3O_8 will cause Pu migration toward the cubic phase. This in turn will cause a decrease in the lattice parameter of the latter. It was also observed by Markin and Street, with a difference in lattice parameters of the M_4O_9 when in equilibrium with M_3O_8 (O/M = 2.307) and with MO_{2+x} (O/M = 2.201) for their sample containing 15% Pu (Figure 8), but was neglected in their conclusions.

If we make the assumption about cation migration, it would imply that the impact on the cubic lattice parameter should decrease with increasing Pu content, considering a fixed, low miscibility of Pu in M_3O_8 and the fact that the maximum content of M_3O_8 formed diminishes with Pu addition. This is in agreement with what we observe. The departure for low Pu contents is much more profound than for samples containing larger quantities of this actinide.

Though cation migration has been reported to begin at elevated temperatures in near-stoichiometric samples, experimental results found in literature indicate that high oxygen potential and the resulting hyperstoichiometry (O/M > 2.00) increase the diffusion coefficients of U and Pu in MOX.[34,35] Thus, considering our experimental conditions, we might expect cation diffusion to be possible at the discussed temperatures.

Distinguishing between M_4O_9 and MO_{2+x}. For $y > 0.5$, Dean[36] and Brett Fox[37] found a single fluorite phase below the tie-line joining $UO_{2.5}$ and PuO_2 compositions. For samples aMOX14, aMOX46, aMOX54, and aMOX62 we could not fit the patterns with two cubic phases at any point during the heat treatment. In the case of aMOX14 it was most likely due to the formation of M_3O_8. Nevertheless, for all samples we could observe a decrease in the intensity of the cubic reflections and a widening of the peaks at 573 K. This distortion is the only premise that makes us consider the presence of two phases at the same time. Most likely two phases were only present for samples containing ≤35 mol % Pu, judging from the obtained fits.

It is not clear whether we observed the I-centered M_4O_9 throughout the whole experiment for low Pu contents. It has been shown by neutron diffraction experiments that, upon oxidation to UO_{2+x}, oxygen will be entering the fluorite structure in clusters, instead of single interstitials, what had been thought before. These clusters were first defined as "Willis structures",[22] but their true nature remains a subject of disputes. The defect-affected domains with distinct ordering would then grow, eventually substituting the initial structure and forming a superstructure of the fluorite phase, namely U_4O_9 or M_4O_9, depending on the material. It has been suggested in previous studies that Pu cations, or other impurities, might affect this ordering. It is discussed further in the Stabilization of the Cubic Phases section. Thus, the structure of this phase and its distinct nature remains unresolved.

On the basis of the above discussion we can state that a distinct second high oxygen phase might have been present in our samples with Pu content ≤35 mol %, but it is unclear whether it was the disputed M_4O_9 or not. For higher Pu contents, oxidation caused a departure from stoichiometry of the MO_2 phase, resulting in MO_{2+x}.

Stabilization of the Cubic Phases. From our results, it is clear that the temperature at which the M_3O_8 structure appeared increased with y. Additionally, the reflections associated with this structure got weaker when y rose. The maximum observed weight % of this phase is listed in Table 1, and this value diminished with increasing Pu content.

First of all, if we consider the cation sublattice with Pu and U ions distributed homogeneously, the oxygen interstitials during oxidation will enter the lattice more readily around U as its oxidation state can be up to +6, while Pu remains +4. If we increase the amount of Pu atoms at the expense of U atoms, one can easily deduce that the highest overall O/M the sample can reach under a given atmosphere will diminish. This in turn means that the maximum wt % of the hexagonal phase should diminish with increasing Pu content, which was observed.

Thus, the actinide shifts the oxygen potential of the material so that at each temperature the higher the Pu content, the

dx.doi.org/10.1021/ic501580x | Inorg. Chem. 2014, 53, 12757−12766

lower the O/M under a given atmosphere. If we assume that M_3O_8 forms above a certain O/M, which might also slightly decrease with Pu content, we might conclude that the hexagonal phase should appear at a higher temperature in our experiments.

Another less direct explanation can be found in the literature. Desgranges et al.[21] proposed that the U_4O_9 and U_3O_7 phases are formed by ordering of oxygen defects arranged in cuboctahedra over large atomic distances and the formation of the U_3O_8 phase is strictly connected to this phenomenon. Thus, again, by introducing impurities to the structure, one disrupts this long-range ordering, preventing the formation of the U_3O_7 phase, and retarding the formation of the U_3O_8. This is also in agreement with experimental results found in ref 38, where the authors observed the γ-U_4O_9 phase in spent fuel, and did not find the U_3O_7 phase upon further oxidation. The γ-U_4O_9 phase corresponds to partially disordered U_4O_9.[39] This is in agreement with the observations of McEachern and Taylor.[14] As the hexagonal phase is supposed to form more readily on U_3O_7, the lack of the former will surely affect the formation of the latter.

From Rietveld refinement we have obtained the kinetics of formation of the hexagonal phase with the evolution of the weight % in time.

If we assume that the O/M in the cubic structure remained constant and the change in overall O/M was achieved only by the increase in M_3O_8 wt %, we can compare the obtained data with the work of Tennery Godfrey.[25] The authors conducted several thermogravimetry experiments on differently fabricated MOX samples with Pu/(U + Pu) of 0.2 and 0.25. One part of the experimental campaign comprised a programmed heating with a rate of 5 °C/min, which is comparable to our overall heating rate throughout the heat treatments. The authors found either one or two stages of oxidation, depending on the sample and heating step. The shape of their O/M versus temperature curve (where the temperature is linearly dependent on time) resembles the one we observe in M_3O_8 wt % versus temperature plots in Figures 3−7, only with a shift in temperature which might be caused by different homogeneities of our samples.

Oxygen Potential of the Gas. The assumption that the incorporation of oxygen should occur at all times above 473 K might not be correct, as demonstrated by Tennery and Godfrey[25] with isothermal experiments. It is clear that the lattice parameter will increase due to thermal expansion during the heating stage and that this phenomenon will not change drastically at any moment; i.e., the considered cubic structure will surely not contract upon heating. Conversely, the varying oxygen content might not always produce a decrease in the lattice parameter as it is not entirely clear whether the equilibrium oxygen potential of the gas at the highest temperature corresponds to the highest O/M of the sample. This might be confirmed by the fact that, for most of the studied samples, the M_3O_8 content was found lower at 1773 K than at 1673 K.

Effect of Self-Irradiation. From comparison of our data with Vegard's prediction for U−Pu−O in Figure 9, it was concluded that all the oMOX samples had increased lattice parameters as compared to the value after annealing. This is most certainly caused by radiation induced damage due to long-term storage inside a glovebox. The effect has been described in previous studies.[31,32] The $\Delta a/a_o$ ratios calculated for all Pu contents at room temperature are listed in Table 4 together with the storage time between fabrication and experiments.

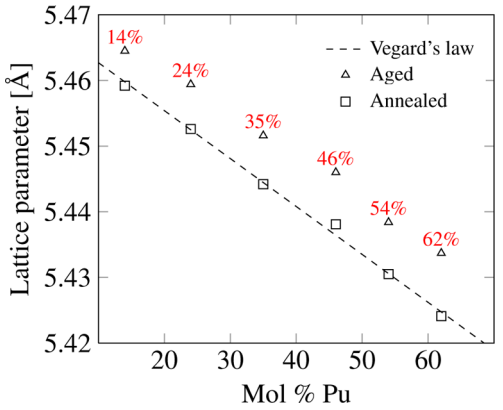

Figure 9. Comparison of the lattice parameters obtained at room temperature for all of our samples before heat treatment with a prediction based on Vegard's law. Lattice parameters of PuO_2 and UO_2 taken from refs 15 and 30.

Table 4. Change Ratio of the Initial Lattice Parameter and Storage Time for All Aged Samples

sample name	$\Delta a/a_o$ [10^{-3}]	Δt storage [days]
oMOX14	0.94	950
oMOX24	1.26	960
oMOX35	1.39	688
oMOX46	1.47	685
oMOX54	1.48	684
oMOX62	1.77	872

If we look at the lattice parameter evolution of the aged samples in Figures 3−7, up to 573 K $\Delta a/a_o$ was observed to be constant. At 573 K, the patterns recorded for all the aged samples were successfully fitted with two cubic phases. Between 573 K and T_r listed in Table 1, which corresponds to the temperature at which the damaged and annealed samples' lattice parameters start to overlap, the difference slowly decreased. At temperatures above T_r, there is little or no difference between the lattice constants, up to a certain point where large amounts of the hexagonal phase cause a departure from linear evolution. The shift of the lattice parameters between the aged and annealed samples MOX24 and MOX54 at temperatures $>T_r$ is most likely due to slight changes in the physical properties of the platinum strip which induced detuning of our temperature regulation. There is no apparent correlation between the history of the sample and the cubic structure lattice parameter evolution after the formation of the hexagonal phase. The fact that two phases were observed at 573 K could be an effect of self-irradiation induced defects that may affect the structural changes the material undergoes during oxidation and cause a slight difference in the low and high oxygen cubic structures for Pu contents above 40 wt %. There is also a possibility that the defects decelerate oxidation and extend the time frame in which two phases could be observed. This would result in exactly what we observe.

In Figure 10 we present the $\Delta a/a_o$ plotted against $\lambda' t$, and compared this to a curve proposed by Kato et al.[16] In the referenced work, the authors conducted XRD measurement during thermal annealing of aged MOX samples and proposed an equation to determine the $\Delta a/a_o$ value of MOX and other

dx.doi.org/10.1021/ic501580x | Inorg. Chem. 2014, 53, 12757−12766

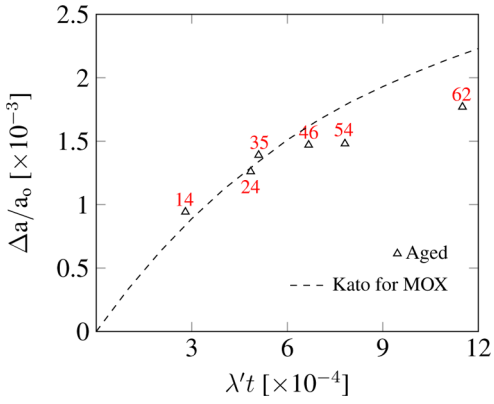

Figure 10. $\Delta a/a_o$ plotted against the effective decay constant λ' multiplied by time, which is proportional to the commonly used displacement per atom unit. Comparison of our data with a curve determined by Kato et al.[16] for MOX with Pu content up to 48.6 wt %.

materials as a function of storage time, isotopic vectors, and constants derived from fitting experimental data. It is as follows:

$$\Delta a/a_o = A[1 - \exp(B \times \lambda' t)] \quad (1)$$

Here A and B are constants, t is time, and λ' is the effective decay constant and is given by

$$\lambda' = C_{Pu} \sum_i \lambda_i C_i \quad (2)$$

where C_{Pu} is the Pu content, λ_i is the decay constant of the Pu isotope, and C_i is the isotopic composition. A and B constants, estimated on the basis of fitting data for materials with different Pu content up to 48 wt %, were estimated to be $A = 2.9 \times 10^{-3}$ and $B = 1.22 \times 10^{-4}$, and the resulting curve is plotted in Figure 10. In our case the storage time from Table 4 and the isotopic composition listed in Table 5 were taken to calculate the corresponding $\lambda' t$ values. A good agreement was found for values up to 46% Pu. It has to be noted though, that Kato et al. chose the A and B constants on the basis of results from samples stored for 15−30 years and around 2 years, with nothing in between. If we closely analyze the values reported by Kato et al. for the samples stored for 600 days, we find a good agreement with our results.

Nevertheless, it is evident that our samples have not reached saturation and the damage level is different in each one; thus, a detailed analysis of influence the amount of defects has on oxidation is not possible. Up to four distict stages of annealing the defects were reported in the literature,[40] but as our samples underwent oxidation during the heat tretment, these processes were surely affected. What is also worth noting is that, through the decay of Pu, small quantities of Am were introduced into both sets of materials. The amounts are around 1.5% (Am/Am + Pu), making it impossible for us to spot the possible effect this has on the oxidation. A dedicated study would be needed to determine whether americium has an impact or not.

CONCLUSIONS

The analysis of diffraction patterns and, in particular, of the evolution of the fluorite structure lattice parameter illustrates that the initial plutonium content has an impact on the oxidation kinetics and products of the studied samples. With the increase in plutonium content, the hexagonal structure appeared at higher temperatures and its maximum observed content diminished. This is most likely caused by changes in the oxygen potential of the material due to the low Pu oxidation state, but the influence of this actinide on the kinetics and nature of crystallographic transitions cannot be neglected.

It was noted that, at temperatures below 473 K, no oxidation occurred, and the samples remained stoichiometric. The incorporation of oxygen began at a temperature between 473 and 573 K for all samples.

We conclude that two cubic phases appear during oxidation for our samples with contents ≤35 mol %. The stoichiometric domain of the high oxygen phase is narrow, and its thermal expansion coefficient is slightly higher than that of MO_2. It was concluded that its lattice constant is unaffected by the changes in the overall O/M when it was observed with small quantities of M_3O_8. For samples with higher Pu contents, the oxidation most likely proceeded by the incorporation of oxygen in the MO_{2+x} lattice, without passing a biphasic domain.

The slight differences in the evolution of the lattice parameter of the aged samples prove that self-irradiation induced defects have an impact on the oxidation kinetics of MOX. One effect of such defects being present in the lattice was found to be a decrease in the oxidation kinetics.

For samples with 14 mol % Pu, large quantities of the hexagonal phase formed at low temperatures and caused significant swelling of the powder. This made the analysis of the cubic phase lattice parameter and phase fractions impossible. We estimate thus that the limit of solubility of Pu in the M_3O_8 structure must be slightly below 14 mol %.

For all the studied samples, when large quantities of the hexagonal phase were formed, the lattice parameter of the cubic type structures was affected. A slight decrease in the linear slope was observed for all samples, and in the case of MOX24, a strong drop in the lattice was noted. Two explanations for this can be proposed. First, cation migration could have induced the transfer of Pu from the hexagonal phase to the cubic one, resulting in the lowering of the lattice parameter. It might also be an effect of an increase in the miscibility of oxygen in the cubic structure at higher temperatures.

Table 5. Isotope Ratios of Samples [Isotope/(Pu + Am)] at the Time of Fabrication

	Isotope ratio [%]					
	oMOX14	oMOX24	oMOX35	oMOX46	oMOX54	oMOX62
Pu-238	0.13	0.13	0.13	0.13	0.13	0.13
Pu-239	78.02	78.02	78.04	78.02	78.04	78.02
Pu-240	18.29	18.29	18.29	18.3	18.29	18.29
Pu-241	1.39	1.39	1.34	1.36	1.34	1.33
Pu-242	0.62	0.62	0.62	0.62	0.62	0.62
Am-241	1.54	1.54	1.57	1.57	1.57	1.59

dx.doi.org/10.1021/ic501580x | Inorg. Chem. 2014, 53, 12757−12766

AUTHOR INFORMATION

Corresponding Authors

*E-mail: michal.strach@cea.fr.

*E-mail: renaud.belin@cea.fr. Phone: +33 4 42 25 49 54. Fax: +33 4 42 25 47 17.

Notes

The authors declare no competing financial interest.

REFERENCES

(1) Olander, D. *J. Nucl. Mater.* **2009**, *389*, 1−22.

(2) Markin, T.; Street, R. *J. Inorg. Nucl. Chem.* **1967**, *29*, 2265−2280.

(3) Sari, C.; Benedict, U.; Blank, H. *J. Nucl. Mater.* **1970**, *35*, 267−277.

(4) Truphémus, T.; Belin, R. C.; Richaud, J.-C.; Reynaud, M.; Martinez, M.-A.; Félines, I.; Arredondo, A.; Miard, A.; Dubois, T.; Adenot, F.; Rogez, J. *J. Nucl. Mater.* **2013**, *432*, 378−387.

(5) Russell, L.; Brett, N.; Harrison, J.; Williams, J. *J. Nucl. Mater.* **1962**, *5*, 216−227.

(6) Javed, N. *J. Nucl. Mater.* **1973**, *47*, 336−344.

(7) Guéneau, C.; Dupin, N.; Sundman, B.; Martial, C.; Dumas, J.-C.; Gossé, S.; Chatain, S.; Bruycker, F. D.; Manara, D.; Konings, R. J. *J. Nucl. Mater.* **2011**, *419*, 145−167.

(8) Agarwal, R.; Sen, B.; Venugopal, V. *J. Nucl. Mater.* **2009**, *385*, 112−116.

(9) Yamanaka, S.; Kinoshita, H.; Kurosaki, K. *J. Nucl. Mater.* **2004**, *326*, 185−194.

(10) Serrano, J.; Glatz, J.; Toscano, E.; Papaioannou, D.; Barrero, J.; Coquerelle, M. *J. Alloys Compd.* **1998**, *271273*, 573−576.

(11) Taylor, P.; Wood, D. D.; Duclos, A.; Owen, D. G. *J. Nucl. Mater.* **1989**, *168*, 70−75.

(12) Teixeira, S. R.; Imakuma, K. *J. Nucl. Mater.* **1991**, *178*, 33−39.

(13) Rousseau, G.; Desgranges, L.; Charlot, F.; Millot, N.; Nièpce, J.; Pijolat, M.; Valdivieso, F.; Baldinozzi, G.; Bérar, J. *J. Nucl. Mater.* **2006**, *355*, 10−20.

(14) McEachern, R.; Taylor, P. *J. Nucl. Mater.* **1998**, *254*, 87−121.

(15) Sari, C.; Benedict, U.; Blank, H. *Proc. Symp. Thermodyn. Nucl. Mater. Emphasis Solution Syst.* **1967**, 587−611.

(16) Kato, M.; Komeno, A.; Uno, H.; Sugata, H.; Nakae, N.; Konashi, K.; Kashimura, M. *J. Nucl. Mater.* **2009**, *393*, 134−140.

(17) Dubrovinsky, L. S.; Saxena, S. K. *Phys. Chem. Miner.* **1997**, *24*, 547−550.

(18) *TOPAS V4: General Profile and Structure Analysis Software for Powder Diffraction Data. User's Manual*; Bruker AXS: Madison, WI, 2005.

(19) Cheary, R.; Coelho, A. *J. Appl. Crystallogr.* **1992**, *25*, 109−121.

(20) Rietveld, H. M. *J. Appl. Crystallogr.* **1969**, *2*, 65−71.

(21) Desgranges, L.; Baldinozzi, G.; Rousseau, G.; Nièpce, J.-C.; Calvarin, G. *Inorg. Chem.* **2009**, *48*, 7585−7592.

(22) Willis, B. *J. Chem. Soc., Faraday Trans. 2* **1987**, *83*, 1073−1081.

(23) Conradson, S. D.; Manara, D.; Wastin, F.; Clark, D. L.; Lander, G. H.; Morales, L. A.; Rebizant, J.; Rondinella, V. V. *Inorg. Chem.* **2004**, *43* (22), 6922−6935.

(24) Belbeoch, B.; Piekarski, C.; Pério, P. *Acta Crystallogr.* **1961**, *14*, 837.

(25) Tennery, V. J.; Godfrey, T. G. *J. Am. Ceram. Soc.* **1973**, *56*, 129−133.

(26) Vauchy, R.; Robisson, A-Ch.; Martin, P. M.; Belin, R. C.; Aufore, L.; Scheinost, A. C.; Hodaj, F. *J. Nucl. Mater.* **2015**, *456*, 115−119.

(27) Wiktor, J.; Barthe, M. F.; Jomard, G.; Torrent, M.; Freyss, M.; Bertolus, M. *Phys. Rev. B* **2014**, *90*, 184101.

(28) Lebreton, F.; Martin, Ph. M.; Horlait, D.; Bès, R.; Scheinost, A. C.; Rossberg, A.; Delahaye, T.; Blanchart, P. *Inorg. Chem.* **2014**, *53*, 9531−9540.

(29) Belin, R. C.; Martin, Ph. M.; Lechelle, J.; Reynaud, M.; Scheinost, A. C. *Inorg. Chem.* **2013**, *56*, 2966−2972.

(30) Grønvold, F. *J. Inorg. Nucl. Chem.* **1955**, *1*, 357−370.

(31) Weber, W. J. *Radiat. Eff. Defects Solids* **1984**, *83*, 145−156.

(32) Nellis, W. *J. Inorg. Nucl. Chem.,, Suppl.* **1977**, *13*, 393−398.

(33) Benedict, U.; Sari, C. *Eur. At. Energy Community—EURATOM* **1969**, 4136 e.

(34) Matzke, H. *J. Chem. Soc., Faraday Trans. 2* **1987**, *83*, 1121−1142.

(35) Berzati, S.; Vaudez, S.; Belin, R. C.; Lechelle, J.; Marc, Y.; Richaud, J.-C.; Heintz, J.-M. *J. Nucl. Mater.* **2014**, *447*, 115−124.

(36) Dean, G. *Proc. Int. Conf. Plutonium, 3rd* **1965**, 806−827.

(37) Brett, N.; Fox, A. *J. Inorg. Nucl. Chem.* **1966**, *28*, 1191−1203.

(38) Thomas, L.; Einziger, R.; Buchanan, H. *J. Nucl. Mater.* **1993**, *201*, 310−319.

(39) Blank, H.; Ronchi, C. *Acta. Crystallogr., Sect. A: Cryst. Phys., Diffr., Theor. Gen. Crystallogr.* **1968**, *A 24*, 657−666.

(40) Staicu, D.; Wiss, T.; Rondinella, V. V.; Hiernaut, J. P.; Konings, R. J. M.; Ronchi, C. *J. Nucl. Mater.* **2010**, *397*, 8−18.